Jusami
Homepage: http://jusami.batan.go.id
Jurnal Sains Materi Indonesia
Akreditation No : 21/E/KPT/2018
Date 9 July 2018
ISSN 1411-1098
E-ISSN 2614-087X

ELECTROCHEMISTRY STUDY ON THE RELATIONSHIP BETWEEN GRAIN BOUNDARY STATE AND CORROSION BEHAVIOR OF ULTRAFINE GRAINED IRON CHROMIUM ALLOY

A D Prasetya[1], M Rifai[1*], A H As'ari[1], Mujamilah[1] and H Miyamoto[2]
[1]Center for Science and Technology of Advanced Material - BATAN
Kawasan Puspiptek, Serpong 15314, Tangerang Selatan
[2]Department of Mechanical Engineering - Doshisha University
Kyoto
E-mail: iamrifai@yahoo.com

Received: 22 August 2019 *Revised: 11 October 2019* *Accepted: 25 October 2019*

ABSTRACT

ELECTROCHEMISTRY STUDY ON THE RELATIONSHIP BETWEEN GRAIN BOUNDARY STATE AND CORROSION BEHAVIOR OF ULTRAFINE GRAINED IRON CHROMIUM ALLOY. Research on stainless steel corrosion resistance continues to grow today. This reality cannot be separated from the needs of stainless steels in various fields, one of which is bio-implant. In this research, the effect of grain size on the corrosion behavior of iron-chromium (Fe-Cr) alloy was investigated. Coarse grain Fe-Cr alloy was first processed with equal channel angular pressing (ECAP) for eight cycles to obtain ultrafine grain structure. The coarse and ultrafine grain samples then were then tested using X-ray Diffractometer (XRD), Scanning Electron Microscope - Electron Backscatter Diffractometer (SEM-EBSD), and the pitting corrosion properties tested using potentiodynamic polarization method in NaCl 1 M solution. The result of XRD dan SEM-EBSD shows that the initial sample is truly has a coarse grain structure with the crystallite size of 48.06 nm, while ECAP produces an ultrafine grain structure with the crystallite size of 31.51 nm. Corrosion test results showed that the ultrafine grain sample had better pitting corrosion resistance compared to the coarse grain sample, with the value of pitting potential for coarse grain sample -0.273 V and 0.386 V for ultrafine grain sample. This behavior is related to the rate of passivation that depends on non-equilibrium grain boundaries, which can be easily observed in the ultrafine grain structure. Based on these results, it can be concluded that the ultrafine grain Fe-Cr alloy has a better corrosion resistance compared to the coarse grain.

Keywords: Pitting corrosion, Stainless steel, ECAP, Ultrafine grain

ABSTRAK

STUDI ELEKTROKIMIA MENGENAI HUBUNGAN ANTARA BATAS BUTIR DAN PERILAKU KOROSI DARI *ULTRAFINE GRAIN* PADUAN LOGAM BESI-KROMIUM. Riset mengenai resistensi korosi *stainless steel* masih terus berkembang sampai saat ini. Hal ini tidak lepas dari kebutuhan *stainless steel* di berbagai bidang, diantaranya bioimplan. Pada penelitian ini telah dilakukan studi mengenai pengaruh ukuran *grain* terhadap perilaku korosi sumuran dari paduan logam besi-kromium (Fe-Cr). Paduan logam besi-kromium dengan struktur *coarse grain* mula-mula diproses dengan *equal channel angular pressing* (ECAP) sebanyak 8 siklus untuk mendapatkan struktur *ultrafine grain.* Sampel *coarse grain* dan *ultrafine grain* lalu diuji menggunakan *X-ray Diffractometer* (XRD), *Scanning Electron Microscope - Electron Backscatter Diffractometer* (SEM-EBSD), dan polarisasi potensiodinamik dalam larutan NaCl 1 M untuk mengetahui sifat korosi sumurannya. Hasil XRD dan SEM-EBSD yang diperoleh menunjukkan bahwa proses sampel awal memang memiliki struktur *coarse grain* dengan ukuran kristalit sebesar 48.06 nm dan proses ECAP menghasilkan struktur *ultrafine grain* sebesar 31.51 nm. Hasil uji korosi menunjukkan bahwa sampel *ultrafine grain* memiliki ketahanan yang lebih baik terhadap korosi sumuran dibandingkan dengan sampel *coarse grain,* dengan nilai tegangan korosi sumuran sebesar -0.273 V untuk sampel *coarse grain* dan 0.386 V untuk *ultrafine grain*. Hal ini tidak lepas dari laju pembentukkan lapisan pasif yang bergantung pada keberadaan *non-equilibrium grain*

boundaries, yang mudah dijumpai pada struktur *ultrafine grain*. Berdasarkan hasil tersebut dapat disimpulkan bahwa paduan logam *ultrafine grain* Fe-Cr memiliki ketahanan korosi sumuran yang lebih baik dibandingkan dengan *coarse grain*.

Kata kunci: Korosi sumuran, *Stainless steel*, ECAP, *Ultrafine grain*

INTRODUCTION

Stainless steel now has been used widely in biomedical applications, especially for implants. Among its uses as implants are for orthopedics, teeth and cardiovascular. Stainless steel has the corrosion resistance property, that is useful for human tissue applications. However, the corrosion resistance of stainless steel is still lower than other metal alloys like Co-Cr, CP titanium or nitinol, so generally, the stainless steel as an implant is only for temporary use [1-3].

Stainless steel is a metal alloy with a minimum Cr content of 10.5% of the overall mass. Based on its composition, stainless steel can be classified into three types, namely austenitic (Fe-Cr-Ni with C content <0.1%), ferritic (Fe-Cr with C content <0.1%), martensitic (Fe-Cr with C content> 0.1%) and duplex.

Cr-Ni austenitic and Cr ferritic are the types that have the best corrosion resistance among the four types [4-6]. The corrosion resistance of stainless steel depends directly on the concentration of Cr metal [2]. The Cr metal can form a passive layer surface that can inhibit the rate of corrosion. A study by Yu et al., 2018 [4] shows that stainless steel with a high Cr content (24%) produces the best corrosion resistance because the passive layer formed is more stable. However, using too much Cr can reduce the economic value of stainless steel because Cr price is higher than Fe. Also, the presence of high content of Cr can trigger intergranular corrosion caused by Cr depletion (thinning) in grain boundaries [7]. Based on this fact, the development of ferritic type stainless steel with low Cr content and better corrosion resistance properties is still needed.

One way to maintain corrosion resistance properties without increasing the Cr metal content in stainless steel is through grain refinement by severe plastic deformation (SPD) method [6, 8]. SPD is a method for obtaining ultrafine-grain structure by reducing material grain size until the sub-micrometer level. Changes in microstructure and mechanical properties after SPD on metals have come to the attention of many researchers. Researches show that microstructure changes affect the corrosion process that occurs [9].

One of the commonly used SPD methods is equal channel angular pressing (ECAP). In the ECAP method, the metal material is pressed through channels at certain angles; as a result, there will be a uniform shift (shear) throughout the entire material [8]. Many studies have shown that the ECAP process increases the corrosion resistance of a metal due to changes in the microstructure of the metal [9-14].

Rifai et al., 2018 [14] compared pitting corrosion resistance of ultrafine grained (UFG) Fe-Cr (8% and 10% Cr content) from SPD process and coarse grain (CG) Fe-12% Cr in NaCl solution 0.6 M. The result showed that the UFG sample had better corrosion resistance than CG, even though it has a lower Cr content. Zheng et al., 2010 [13] also compared the corrosion resistance of commercial stainless steel 304 (SS 304) and SS 304 that had been ECAP in 0.5 M H2SO4 solution. The results showed that SS 304, which had been through the ECAP cycle process four and eight times showed better corrosion resistance than the commercial SS 304. However, making UFG especially with the ECAP process will reduce the formability and ductility of the material. To re-improve, these characteristics, the annealing process is generally carried out [15]. Various studies on the method of heat treatment through annealing show that the defects of metal can decrease [15,16].

The focus of this research is on the study of chemical processes related to corrosion that occurs due to changes in grain size due to the ECAP process in Fe-Cr metal alloys with a Cr content of 20%. The use of Cr, which reaches 20%, is based on the corrosion rate, which rapidly will increase if it is below 20% and less significant corrosion rate above 20% [17]. In addition to the corrosion process that occurs, the process of forming a passive layer that occurs also becomes the focus of discussion because the formed passive layer influences the type of corrosion and the rate of corrosion that occurs.

EXPERIMENTAL METHOD

Materials and Instruments

The materials used in this study are Fe-Cr metal alloys with very low carbon (C) and nitrogen (N) content (Cr; 20.03%, C; 0.0004% N; 0.0013%, and Fe 79.9683% in mass percent), high temperature lubricant made from fluorine, NaCl 1 M solution, etching solution and argon gas, sandpaper no. 240-2000, and buff paper with alumina suspension (PRESI) 9 μm, 3 μm, and 1 μm, OP-S suspension (Streuers).

The tools used in this study include an ECAP machine, a spark-erosion machine, Field emission-scanning electron microscopy (FE-SEM; JSM 7001F) equipped with electron backscatter diffraction (EBSD, Oxford Instruments Co .: Model: HKL) and software image processor EBSD INCATM (Oxford Instruments

Co.), X-Ray Diffractometer (SmartLab, Rigaku), and potentiostat (HOKUTO H100) with Ag/AgCl reference electrodes.

Method and Procedure

Initial coarse grain specimens were formed with dimensions of 8 × 8 × 120 mm. The sample then processed by ECAP, eight cycles at 423 K via Bc route using a split die with two channels intersecting at an angle of 90° to obtain an ultrafine grain structure, the specimen was then lubricated with high-temperature fluorine-based lubricants. Initial and after ECAP specimens were then prepared using a spark-erosion machine. The tested specimens have a square shape with an area of 8 mm × 6 mm and a thickness of 2 mm. The specimens which corrosion test is done is connected by wire at the back of the side surface using solder and coated with epoxy molding to cover the connection. The side edge of the specimen is covered with tape to prevent corrosion caused by side effects from pitting corrosion. The connected specimens were then grounded using sandpaper no. 240 to 2000, then polished with buff paper with 9 μm alumina suspension, 3 μm, and 1 μm. In the last stage of polishing, OP-S suspension is used.

Coarse grain and ultrafine grain specimens were characterized using Field-emission scanning electron microscopy (FE-SEM) with electron backscatter diffraction (EBSD) and X-ray Diffractometer (XRD).

FE-SEM EBSD is used to determine the orientation map of samples, and XRD is used to determine the phase of the sample. The image obtained from EBSD is then processed using INCA software.

Anodic corrosion polarization tests were carried out in NaCl 1 M solution at room temperature with potentiodynamic polarization using a potentiostat with a scan rate of 20 mV/min, corrosion current and Ag / AgCl reference electrodes recorded with a data logger. Each sample is then dipped in the etching solution for 1 hour. Before the anodic corrosion polarization test was carried out, the solution was flushed with argon gas to remove dissolved oxygen. The polarization test process begins after the open circuit potential (OCP) of the specimen has been stabilized. Polarization starts at 50 mV, lower than OCP after immersion in the test solution for 5 minutes.

RESULT AND DISCUSSION

In the diffractogram shown in Figure 1. the ultrafine grain sample from ECAP has broader peaks than the coarse grain sample. This diffractogram does not only show differences in grain size but also shows the effect of ECAP. The ECAP process produces an ultrafine grain structure in the presence of high non-equilibrium grain boundaries, whereas sample before ECAP has a coarse grain structure in the presence of higher

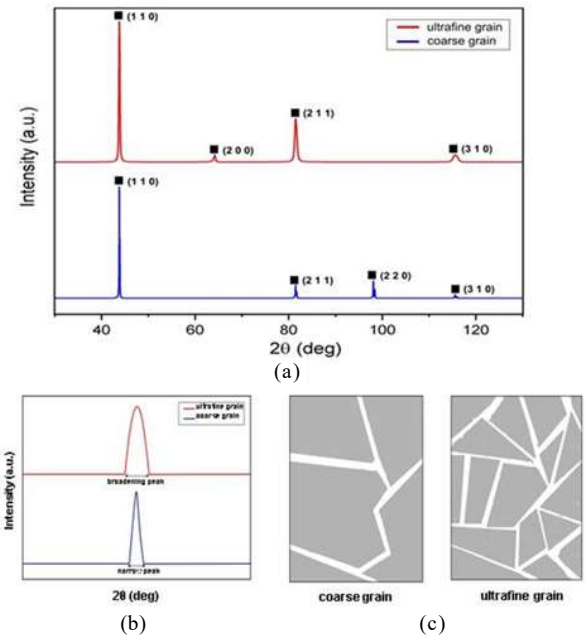

Figure 1. (a). Diffraction patterns of coarse grain and ultrafine grain samples, (b). illustration of peak broadening in diffraction patterns, (c). different grain size schemes of coarse grain and ultrafine grain structures.

equilibrium grain boundaries. The presence of high non-equilibrium grain boundaries in the ul-trafine grain structure increases the density of free energy, increase the width and the density of disloca-tions [8, 17]. The high density of free energy in these non-equilibrium grain boundaries will increase the rate of diffusion from inside the material grains [18].

Based on the diffractogram (Figure 1a), there are three similar peaks appearing on both dif-fractograms. The first peak located at 43.8 ° is from α-Fe (1 1 0), the second peak at 81.5 ° is from α-Fe (2 1 1) peak, and the third peak at 115.5 ° is from Fe (3 1 0). The peaks at 64 ° and 98 ° also still belong to α-Fe with the plane orientation of (2 0 0) and (2 0 0) respectively. The diffractogram indirectly shows that the sample is composed of ferritic Fe or α-Fe phases. It can be seen from the diffractogram (Figure 1a) of coarse grain sample that there is a missing peak, but there is also a peak that appears when compared to the diffractogram of ultrafine grain sample. The missing and appearing peaks do not indicate that the two samples have different phases, it is because the ultrafine grain sample has a small size of grain which produce low intensity of diffraction when analyzed using XRD. The diffractogram in Figure 1a confirms the small crystallite size of the ultrafine grain sam-ple, where for the ultrafine grain the peaks are wider than the coarse grain (illustrated in Figure 1b) and also by calculating the crystallite size on both sam-ples using Scherrer's equation at 2θ 43.8° (the peak with the highest intensity), the coarse grain sample has a crystallite size of 48 nm, while the ultrafine grain only 31.5 nm. As a result, various distribution of grains with various kinds

of plane orientation for the ultrafine grain was obtained (shown from EBSD data).

The two samples can be compared only from differences in grain size because there is no phase difference between the two. The emergence of a new peak in the ultrafine grain diffractogram is due to many grains that appear. The grains seem to have a different orientation so that it will be detected as a new peak in the XRD, without phase changes.

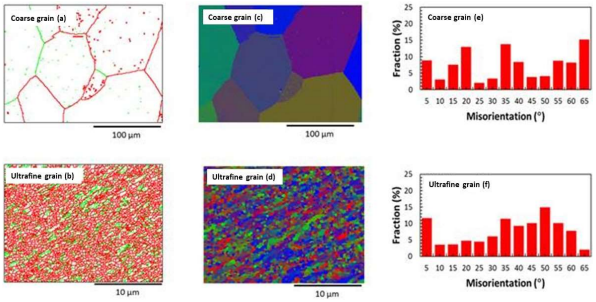

Figure 2. SEM-EBSD coarse grain and ultrafine grain results grain boundary images (a). coarse grain, (b). ultrafine grain; orientation images (c). coarse grain, (d). ultrafine grain; misorientation distribution graphs (e). coarse grain, (f). ultrafine grain

The EBSD results presented in Figure 2. strengthen the XRD data. EBSD results show that the ECAP process produces an ultrafine grain structure, while the initial sample has a coarse grain structure. The ultrafine grain sample has a fraction with misorientation (defects) above an angle of 35° and grain boundaries more than the coarse grain sample. Thus, both samples structures only have differences in grain size and defects (which is a consequence of grain size).

Samples	E_{pit} (V)	E_{pp} (V)	$I_{passive}$ (mA.cm^2)	I_{crit} (mA.cm^2)
Ultrafine grain	0.386	0.071	0.1	0.068
Coarse grain	-0.273	-	-	-

Miyamoto, 2016 [19] and Ralston et al., 2010 [12] suggested that the corrosion behavior of a metal material depends on the grain size. In general, the local corrosion rate (such as pitting or intergranular corrosion) will decrease in line with the smaller grain size. It is in line with differences in the pattern of anodic polarization curves obtained, which are presented in Figure 3. In the curve the coarse grain sample has a pitting potential (E_{pit}) around -0.273 V vs Ag/AgCl 3 M, while ultrafine grain the corrosion starts occurred at E_{pit} 0.386 V vs Ag/AgCl 3 M. The results of the curve showed that the ultrafine grain sample has better corrosion resistance than the coarse grain sample [8, 18]. Excellent resistance to pitting corrosion cannot be separated from the influence of grain size on passive layer formation.

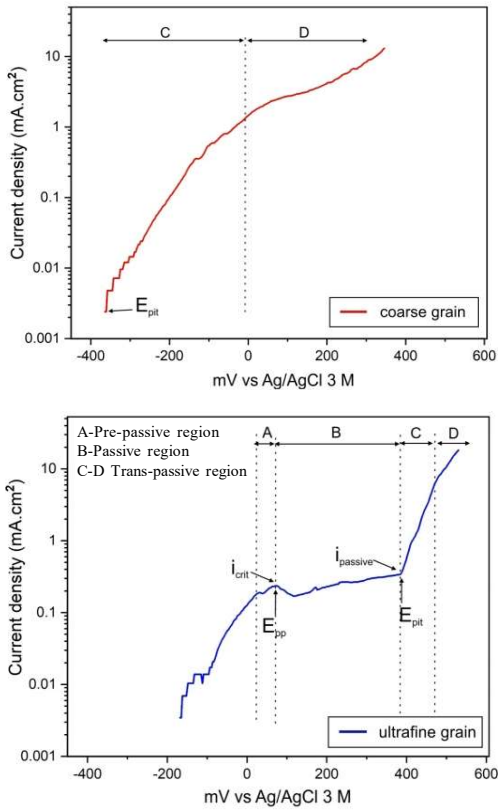

Figure 3. Comparison of coarse grain polarization curve

The polarization curve results obtained (Figure 3) can be interpreted into three parts for the ultrafine grain sample and one part for the coarse grain sample [20,21]. On the ultrafine grain polarization curve, there are pre-passive region, passive region, and trans-passive region, whereas on coarse grain polarization curves only trans-passive region can be obtained. Also, the curve can be identified as passive potential (E_{pp}), pitting potential (E_{pit}), passive current ($i_{passive}$), and maximum anodic dissolution current from ultrafine grain sample, while from coarse grain sample only pitting potential can be obtained. Based on the polarization curve data, passivation occurs at the ultrafine grain sample, indicated by the presence of a passive region before reaching E_{pit}. Whereas in the coarse grain sample polarization curve, the passive region cannot be identified although the trans-passive region (or pitting region) can be identified. Based on this, the formation of a passive layer in the coarse grain sample cannot be justified from the anodic polarization curve data. However, according to Rifai et al., 2015 [8] before pitting corrosion occurs, there was a formation of a passive layer. In general, the passive layer corrodes metal at a slow rate throughout the surface so sometimes corrosion tends to be concentrated in one part, which consequently can cause local corrosion, more specifically such as pitting corrosion.

The formation of a passive layer in stainless steel containing Cr generally follows the theory of the formation of an oxide layer. The formation of a passive layer itself involves ion transfer (anions and cations) or charge transfer at the surface of the passive metal-layer interface (oxide layer) and the interface of the passive-electrolyte layer [22-24]. Ion transfer occurs through (cations or anions) vacancies; this means defects in the oxide layer are needed. Ion transfer to the oxide layer occurs because of the presence of an electric field due to the potential difference between the metal and the solution [23].

The ion transfer is also affected by grain size. Smaller grain size increases the rate of diffusion of Cr^{3+} ions towards the outermost layer. It is due to ultrafine grain (smaller grain size) besides having high grain boundaries density, it also has more fractions and defects on the surface [6,25]. An illustration of the diffusion scheme that occurs is presented in Figure 4.

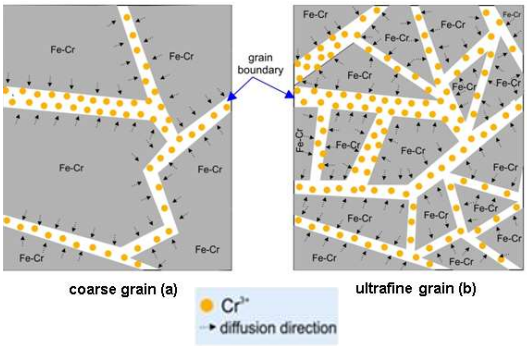

Figure 4. Comparison of coarse grain diffusion illustrations with the ultrafine grain. In the ultrafine grain sample, the Cr3+ diffuse from the internal structure is more massive because of the large number of grain boundaries.

On the other hand, the presence of water molecules in the environment, as well as the influence of a strong electric field, also causes water anions from the environment to migrate/diffuse in the outer layers of metal (film). On the outer surface of the metal, Cr^{3+} ions will react with oxygen and water anions and form a thin layer of Cr_2O_3 on the surface of the material or commonly called as passive layer [22,25,26]. Overall, the ultrafine grain structure increases the diffusion of Cr^{3+} ions on the surface so that the passive layer will be thicker and more stable. The passivation process is illustrated in Figure 5

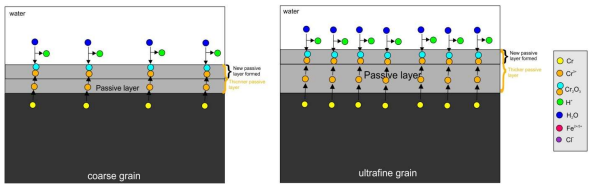

Figure 5. Comparison of illustrations of coarse grain formation with the ultrafine grain. In a sample of ultrafine grain, the passive layer is formed thicker due to the diffusion of Cr3+ to the surface is more massive.

and the reaction of the formation of the passive layer in equations 1-4.

$$Cr \rightarrow Cr^{3+}_{(ox)} + 3e^- \quad \text{..... (1)}$$

(reaction occurs at the metal-passive layer interphase)

$$Cr^{3+}_{(ox)} \rightarrow Cr^{3+}_{(aq)} + 3e^- \quad \text{..... (2)}$$

(reaction occurs at the passive layer-electrolyte solution interphase)

$$O^{2-}_{(ox)} + 2H^{+}_{(aq)} \leftrightarrow 2H_2O \quad \text{..... (3)}$$

(reaction occurs at the passive layer-electrolyte solution)

$$2Cr^{3+}_{(ox)} + 3O^{2-}_{(ox)} \rightarrow Cr_2O_{3(ox)} \quad \text{..... (4)}$$

(formation and thickening of the passive layer)

As previously explained, based on polarization curves data, the ultrafine grain sample has better resistance to pitting corrosion than the coarse grain sample. Pitting corrosion is a localized corrosive attack of a passive metal that can form small cavities (pits). Pitting corrosion requires the presence of aggressive anions (generally chloride ions) and oxidizing agents such as oxygen or ferric ions [6, 22]. In pitting corrosion, oxidation-reduction reactions occur. The oxidation reaction takes place in the pit (hole) that is formed. This reaction will release metal ions, and electrons, where metal ions will dissolve in solution, and electrons will migrate to the cathode through the metal (equation 5). The presence of water will cause a further reaction, namely oxidation, and formation of rust (Fe_3O_4) (equation 6). The oxygen reduction reaction itself takes place on the metal surface (cathode) (equation 7) [26]. The reaction does not only occur with Fe but also applies to Cr. If a passive layer is formed, oxidation from the passive layer occurs first. Therefore, the resistance and thickness of the passive layer are essential in preventing pitting corrosion.

$$Fe_{(s)} \rightarrow Fe^{2+}_{(aq)} + 2e^- \quad \text{..... (5)}$$

$$3Fe^{2+}_{(aq)} + 4H_2O \rightarrow Fe_3O_{4(s)} + 8H^{+}_{(aq)} + 2e^- \quad \text{.... (6)}$$

$$O_2 + 2H_2O + 4e^- \rightarrow 4OH^- \quad \text{..... (7)}$$

Once Fe in the metal dissolves as Fe^{2+} ions and forms rust, then further corrosion will run quickly. The process of continued corrosion will also be faster because of the autocatalytic process due to the presence of chloride ions [17,27]. As a result, the pit formed will be deeper and broader. The autocatalytic process of Fe metal dissolution due to Cl^- ions is presented in equation 9-10, and for Cr metal in equation 11-14. An illustration of the pitting corrosion scheme that occurs in ultrafine grain and coarse grain samples is presented in Figure 6.

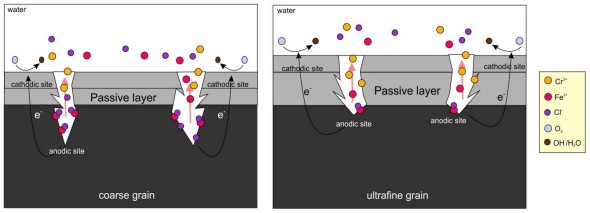

$$Fe_{(s)} \rightarrow Fe^{2+}_{(aq)} + 2e^- \quad \text{..... (8)}$$

(hydrolysis of Fe, same as reaction 5 for Cr)

$$[Fe(Cl)]_{ads} \rightarrow [Fe(Cl)]^{+}_{(aq)} + e^- \quad \text{..... (9)}$$

(Fe dissolving because of Cl^- ions attack)

$$[Fe(Cl)]^{+}_{(aq)} + H^+ \rightarrow Fe^{2+}_{(aq)} + HCl \quad \text{..... (10)}$$

$$Cr_{(s)} + 2Cl^-_{(aq)} \rightarrow [CrCl_2]_{ads} + 2e^- \quad \text{..... (11)}$$

$$Cr_{(s)} + 3Cl^-_{(aq)} \rightarrow [CrCl_3]_{ads} + 3e^- \quad \text{..... (12)}$$

$$[Cr(Cl)_n]_{ads} \rightarrow [Cr(Cl)_n]^{n+}_{(aq)} + ne^- \quad \text{..... (13)}$$

$$[Cr(Cl)_n]^{n+}_{(aq)} + nH^+ \rightarrow Cr^{n+}_{(aq)} + nHCl \quad \text{..... (14)}$$

CONCLUSION

Pitting corrosion behavior of Fe-Cr metal alloys depends on the grain structure. It is because the grain structure has an influence on the diffusion of Cr^{3+} ions from the internal structure, which has a direct impact on the passive layer that is formed. In the ultrafine grain structure, many grain boundaries are formed, so that the diffusion of the Cr^{3+} ions will run more massive and faster, whereas for coarse grain structures the opposite happens. The thicker and more stable the passive layer is formed, the better the resistance of material from pitting corrosion. Fe-Cr metal alloy from ECAP has an ultrafine grain structure while the initial sample has a coarse grain structure, so the ultrafine grain sample has better resistance than coarse grain.

ACKNOWLEDGMENT

We would like to thank Center for Science and Technology of Advanced Materials, National Nuclear Agency and Department of Mechanical Engineering, Doshisha University for providing the research facilities.

REFERENCES

[1]. I. Gotman, "Characteristics of Metals Used in Implants" *J. Endourol.*, vol. 11, no. 6, pp. 383–389, 2009.

[2]. L. D. Zardiackas, "Stainless Steels for Implants," *Wiley Encycl. Biomed. Eng.*, 2006.

[3]. N. Godbole, S. Yadav, M. Ramachandran, and S. Belemkar, "A review on surface treatment of stainless steel orthopedic implants," *Int. J. Pharm. Sci. Rev. Res.*, vol. 36, no. 1, pp. 190–194, 2016.

[4]. Y. Yu, S. Shironita, K. Souma, and M. Umeda, "Effect of chromium content on the corrosion resistance of ferritic stainless steels in sulfuric acid solution," *Heliyon*, vol. 4, no. 11, p. e00958, 2018.

[5]. N. J. Den Uijl and L. J. Carless, "Advanced metal-forming technologies for automotive applications," *Adv. Mater. Automot. Eng.*, pp. 28–56, 2012.

[6]. R. K. Gupta and N. Birbilis, "The influence of nanocrystalline structure and processing route on corrosion of stainless steel: A review," *Corros. Sci.*, vol. 92, pp. 1–15, 2015.

[7]. X. Li, Y. Ni, Y. Jiang, J. Li, and L. Li, "Intergranular Corrosion of Low Cr Ferritic Stainless Steel 429 Evaluated by the Optimized Double Loop Electrochemical Potentiokinetic Reactivation Test," *Adv. Mater. Sci. Eng.*, vol. 2015, pp. 1–10, 2015.

[8]. M. Rifai, H. Miyamoto, and H. Fujiwara, "Effects of Strain Energy and Grain Size on Corrosion Resistance of Ultrafine Grained Fe-20%Cr Steels with Extremely low C and N Fabricated by ECAP," *Int. J. Corros.*, vol. 2015, no. 1, pp. 1–9, 2015.

[9]. M. Ilieva and R. Radev, "Effect of severe plastic deformation by ECAP on corrosion behaviour of aluminium alloy AA 7075," *Arch. Mater. Sci. Eng.*, vol. 81, no. 2, pp. 55–61, 2016.

[10]. G. Song, *Corrosion behavior of magnesium alloys and protection techniques*, vol. 2. Woodhead Publishing Limited, 2010.

[11]. K. Gopala Krishna, K. Sivaprasad, T. S. N. Sankara Narayanan, and K. C. Hari Kumar, "Localized corrosion of an ultrafine grained Al-4Zn-2Mg alloy produced by cryorolling," *Corros. Sci.*, vol. 60, pp. 82–89, 2012.

[12]. K. D. Ralston, N. Birbilis, and C. H. J. Davies, "Revealing the relationship between grain size and corrosion rate of metals," *Scr. Mater.*, vol. 63, no. 12, pp. 1201–1204, 2010.

[13]. Z. J. Zheng, Y. Gao, Y. Gui, and M. Zhu, "Optimization of Strength and Ductility in Ultra-Fine 304 Stainless Steel after Equal-Channel Angular Processing," *Mater. Sci. Forum*, vol. 667–669, pp. 937–942, 2010.

[14]. M. Rifai, M. Yuasa, and H. Miyamoto, "Enhanced Corrosion Resistance of Ultrafine-Grained Fe-Cr Alloys with Subcritical Cr Contents for Passivity," *Metals (Basel).*, vol. 8, no. 3, p. 149, 2018.

[15]. O. Saray, G. Purcek, I. Karaman, and H. J. Maier, "Improvement of formability of ultrafine-grained materials by post-SPD annealing," *Mater. Sci. Eng. A*, vol. 619, pp. 119–128, 2014.

[16]. J. Niehuesbernd, E. Bruder, and C. Müller, "Impact of the heating rate on the annealing behavior and resulting mechanical properties of UFG HSLA

steel," *Mater. Sci. Eng. A*, vol. 711, pp. 325–333, 2018.

[17]. P. Fauvet, "Corrosion issues in nuclear fuel reprocessing plants," *Nucl. Corros. Sci. Eng.*, pp. 679–728, 2012.

[18]. X. Sauvage, G. Wilde, S. V. Divinski, Z. Horita, and R. Z. Valiev, "Grain boundaries in ultrafine grained materials processed by severe plastic deformation and related phenomena," *Mater. Sci. Eng. A*, vol. 540, pp. 1–12, 2012.

[19]. H. Miyamoto, "Corrosion of Ultrafine Grained Materials by Severe Plastic Deformation, an Overview," *Mater. Trans.*, vol. 57, no. 5, pp. 559–572, 2016.

[20]. E. McCafferty, *Introduction to Corrosion Science*, 1st ed. New York, NY: Springer New York, 2010.

[21]. N. Mahato, M. H. Cho, and M. M. Singh, "Electrochemical, surface analytical, and spectroscopic study of passive film and pits formation on food grade ferritic stainless steel AISI-430 in aqueous acetic acid containing chloride ions," *Mater. Corros.*, vol. 69, no. 12, pp. 1770–1783, 2018.

[22]. D. Landolt, Corrosion and surface chemistry of metals , Lausanne:EPFL Press, 2007, pp. 1-165

[23]. P. Marcus, É. Protopopoff, and V. Maurice, "Surface Chemistry and Passivation of Metals and Alloys," *Mech. - Microstruct. - Corros. Coupling*, no. Cc, pp. 91–120, 2019.

[24]. C. O. A. Olsson and D. Landolt, "Passive films on stainless steels - Chemistry, structure and growth," *Electrochim. Acta*, vol. 48, no. 9 SPEC., pp. 1093–1104, 2003.

[25]. A. Abbasi Aghuy, M. Zakeri, M. H. Moayed, and M. Mazinani, "Effect of grain size on pitting corrosion of 304L austenitic stainless steel," *Corros. Sci.*, vol. 94, pp. 368–376, 2015.

[26]. I. B. Obot, "Recent Advances in Computational Design of Organic Materials for Corrosion Protection of Steel in Aqueous Media," *Dev. Corros. Prot.*, no. 2010, 2014.

[27]. J. Kang, J. Li, K. Y. Zhao, X. Bai, Q. L. Yong, and J. Su, "Passivation Behaviors of Super Martensitic Stainless Steel in Weak Acidic and Weak Alkaline NaCl Solutions," *J. Iron Steel Res. Int.*, vol. 22, no. 12, pp. 1156–1163, 2015.